International Journal of Minerals, Metallurgy and Materials
Volume 28, Number 12, December 2021, Page 1976
https://doi.org/10.1007/s12613-020-2090-4

Highly efficient nanocatalyst Ni_1Co_9@graphene for hydrolytic dehydrogenation of sodium borohydride

Juan Wang[1,2], *Li-jun Yang*[2], *Xiao-chong Zhao*[2], *Pan Yang*[2], *Wei Cao*[2], *and Qing-song Huang*[1]

1) School of Chemical Engineering, Sichuan University, Chengdu 610065, China
2) Institute of Materials, Chinese Academy of Engineering Physics, Jiangyou 621908, China
(Received: 21 March 2020; revised: 1 May 2020; accepted: 7 May 2020)

Abstract: Bimetal materials derived from transition metals can be good catalyst candidates towards some specific reactions. When loaded on graphene (GP), these catalysts exhibit remarkable performance in the hydrolysis of sodium borohydride. To obtain such catalysts easily and efficiently, a simple thermal reduction strategy was used in this study, and Ni_xCo_{10-x} series bimetal catalysts were prepared. Among all the catalysts, Ni_1Co_9 exhibited the best catalytic performance. The turnover frequency (TOF) related to the total number of atoms within the bimetallic nanoparticles reached 603.82 $mL \cdot mmol^{-1} \cdot min^{-1}$ at 303 K. Furthermore, graphene was introduced as a supporting frame. The Ni_1Co_9@Graphene (Ni_1Co_9@GP) had a large surface area and high TOF, 25534 $mL \cdot mmol^{-1} \cdot min^{-1}$, at 303 K. The Ni_1Co_9@GP exhibited efficient catalytic properties for H_2 generation in alkaline solution because of its high specific surface area. Moreover, the high kinetic isotope effect observed in the kinetic studies suggests that using D_2O led to the oxidative addition of an O–H bond of water in the rate-determining step.

Keywords: transition metal; bimetallic nanocatalyst; sodium borohydride; hydrolysis

1. Introduction

The overexploitation and overuse of sustainable energy have been a concern. Numerous studies have been conducted on high-capacity hydrogen storage materials, such as sodium borohydride ($NaBH_4$) [1–4] and hydrazine monohydrate ($H_2NNH_2\ H_2O$) [5]. Hydrogen storage using sodium borohydride ($NaBH_4$) is one of the most attractive hydrogen storage methods because of the following: (1) $NaBH_4$ is lightweight and occupies a small volume; (2) hydrogen is obtained as the only gaseous product from the hydrolysis reaction; (3) controllable hydrogen production rate; (4) great hydrogen storage capacity (10.8wt%); (5) high stability of $NaBH_4$ in alkaline solution; (6) environment-friendly properties [6–7]. In 1977 [8], alloy nanoparticles (NPs) were first introduced in industrial and fundamental research because of their properties, such as magnetic, optical, and catalytic properties [9–10], which are usually better than those of their corresponding monometallic NPs [11–13]. This concept has been attracting much attention for a long time. Noble metals, such as Pd, Au, and Y, have exhibited remarkable catalytic performance in hydrides such as in the hydrolysis of sodium borohydride [11,14]. However, considering that these metals are too expensive to apply in factories, researchers have started to seek new and cheap catalyst replacements with similar performance. Researchers have found that transition metals, such as Ni, Co, Fe, and Cu, show the potential to replace noble metals. Chen *et al.* [15] indicated that alloying both noble metals and transition metals have advantages in terms of expense and the provision of active sites for synergetic catalysis. Guo and Lu [16] considers it is essential to use only cheap and available materials to replace noble metal catalysts for hydrogen generation methods. Additionally, porous materials are widely used as supports for bimetallic nanocatalysts inhydrolysis, which can enhance the catalytic performance of the bimetallic nanocatalysts [17]. Porous materials, such as graphene [18], carbon nanotubes (CNTs) [19], activated carbon [20], carbon black [21], and graphite [22], have been used for the hydrolysis of $NaBH_4$ solution. Owing to the high surface energy of alloyed nanomaterials, NPs sometimes become inhomogeneously alloyed and easily aggregate [23]. As a result, ultrafine well-alloyed NPs play an important role in modern catalysis, as they make nanocatalysts exhibit their best efficiency [24–25]. Graphene is a supporting material that exhibits excellent electronic, optical, chemical, and mechanical properties and has a large specific

Corresponding author: Qing-song Huang E-mail: qshuang@scu.edu.cn

surface area; these properties make it a suitable support of nanocatalysts. The highly conductive surface and increased surface area of graphene could benefit hydrogen decomposition [26]. Furthermore, graphene can reduce the overall weight of the nanocatalysts due to its light weight. Above all, it acts as a "substrate" on which these bimetal NPs are evenly distributed, while the bimetal NPs are likely to aggregate [27].

In this paper, we report a general and facile method for preparing bimetallic Ni_1Co_9 nanosheet anchored on graphene (Ni_1Co_9@GP). After its preparation, the Ni_1Co_9@GP was used as a catalyst for sodium borohydride ($NaBH_4$) hydrolysis from aqueous alkaline solution. The Ni_1Co_9@GP catalyst exhibited high activity toward the dehydrogenation of $NaBH_4$ at 303 K. It also exhibited superior stability in the durability performance experiment.

2. Experimental

2.1. Chemicals and materials

Nickel nitrate hexahydrate ($Ni(NO_3)_2{\cdot}6H_2O$, 99wt%), cobalt nitrate hexahydrate ($Co(NO_3)_2{\cdot}6H_2O$, 99wt%), sodium hydroxide (NaOH, 98wt%), deuteroxide (D_2O, 99.9wt%), sodium borohydride ($NaBH_4$, 99wt%), and graphene were purchased from Jiangsu XFnano Technology Co., Ltd.. All the chemicals were used as received without further purification. Graphene was used to prepare the graphene suspension with ultrapure water.

2.2. Preparation of Ni_xCo_{10-x} nanocatalysts

20 mg graphene was added to the ultrapure water and was treated by ultrasound for 1 h. Then the $Ni(NO_3)_2{\cdot}6H_2O$ and $Co(NO_3)_2{\cdot}6H_2O$, with molar ratios of 1:9, 2:8, 3:7, 4:6, 5:5, 6:4, 7:3, 8:2, 9:1, were added to the suspension, and the mixture was stirred over 10 h at 600 r/min. Finally, a thoroughly mixed solution was obtained. To reduce the transition metal salt, 5 mmol $NaBH_4$ was added to the solution, and the solution was left to stand for 0.5 h. The solution was centrifuged four times, and precipitation was obtained. Finally, sample was then freeze-dried to obtain the final catalyst.

2.3. Characterization

The crystal structures of Ni_xCo_{10-x} were examined by X-ray diffraction (XRD) with Cu K_α radiation. The morphological characteristics of the catalyst were confirmed by transmission electron microscopy (TEM). X-ray photoelectron spectroscopy (XPS) with Al K_α radiation was used to study the chemical state of the Ni_xCo_{10-x} catalyst. Nitrogen adsorption–desorption isotherms were obtained by a Quantachrome surface area analyzer at 77.3 K. Before adsorption, all catalysts were degassed under vacuum at 348 K for 8 h. Pore size distributions were obtained via the Brunauer–Emmett–Teller method using the desorption branch of the isotherm. The samples were dried overnight at 200 K in a vacuum freeze dryer before the test. Approximately 100 mg of the sample was filled into glass ampoules and then outgassed in high vacuum at 323 K for 5 h before the test.

A specific amount of Ni_xCo_{10-x} nanocatalyst was added to the NaOH solution (1 M, 1.5 mL), and then the suspension was thoroughly stirred for 15 min at 30°C. The calculated $NaBH_4$–NaOH solution was quickly added to the suspension. Different from the typical experiment using hydrous hydrazine as hydrides, only one reaction occurs in this experiment, as shown in Eq. (1):

$$NaBH_4 + (2+x)H_2O \xrightarrow{\text{Catalyst}} NaBO_2 \cdot xH_2O + 4H_2,\ \Delta H = -248.9\ \text{kJ/mol} \quad (1)$$

2.4. Catalytic tests

The hydrolysis of $NaBH_4$ occurs in an alkaline environment. Because of the highly deliquescent characteristic of $NaBH_4$, it was always added into NaOH solution (1 M) in a concentration of 1 mmol per 200 μL and stirred adequately before it was added to the Ni_1Co_9@GP–NaOH suspension. Additionally, the $NaBH_4$–NaOH aqueous solution needs to be freshly prepared and used on the same day. The nanocatalyst and NaOH aqueous solution were added into a three-necked flask. Under a certain temperature, the hydrolysis of $NaBH_4$ started immediately, and hydrogen was collected by the drainage gas collection method. The durability performances of the Ni_xCo_{10-x} catalysts were tested: the catalyst with the best performance among the samples was chosen to be used eight cycles at 303 K in NaOH solution (1 M, 1.5 mL). After the first cycle of hydrolysis, the equivalent amount of $NaBH_4$–NaOH solution was added into the three-necked flask. The turnover frequency (TOF) can be obtained according to Eq. (2). The TOF is a measurement of the reaction rate of a catalyst, which represents the intrinsic activity of the catalyst.

$$\text{TOF} = \frac{V_{H_2}}{n_{\text{catalyst}} \cdot t} \quad (2)$$

where V_{H_2} denotes H_2 volume; n_{catalyst} denotes molar mass of catalyst; t denotes minutes of hydrolysis.

According to Eq. (1), $NaBH_4$ provides only four hydrogen atoms to the final product H_2. Herein, a method in which D_2O replaces H_2O in the hydrolysis was introduced, so that NaOH–D_2O solution (1 M, 1.5 mL) and $NaBH_4$–NaOH–D_2O solution were used. The amount of H_2 collected by the measuring cylinder can indicate whether another hydrogen atom came from H_2O. In addition, the reaction kinetics was studied based on the logarithmic plot of the H_2 generation rate vs. the concentration of Ni_1Co_9@GP and is discussed in the subsequent section.

3. Results and discussion

Compared with Ni_xCo_{10-x}, when Ni or Co acts as a catalyst

in hydrolysis, a higher temperature of at least 333 K is needed due to their lower catalytic activity. Fig. 1 shows that the TOF value of Ni_xCo_{10-x} decreases with the increase in x. This proves that the more the amount of Co in the catalyst, the better the catalytic performance. The hydrolysis of $NaBH_4$ was conducted in water at 303, 313, and 323 K with 0.39 mmol nanocatalyst. The hydrolysis happened slowly at room temperature, while beyond 323 K, the reaction was extremely fierce that it is not easy to statistically quantify. The TOF values of all the hydrolysis reactions of $NaBH_4$ using Ni_xCo_{10-x}@GP as catalyst were calculated and are given in Fig. 1. By comparing the TOF values from eight kinds of Ni_xCo_{10-x} catalysts at different temperatures, a conclusion can be drawn that Ni_1Co_9 had the best performance.

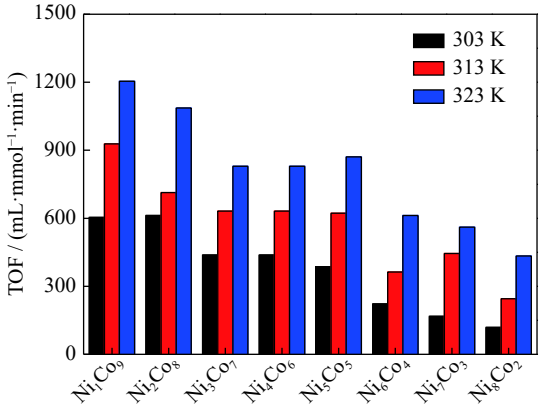

Fig. 1. Comparison of the TOF values of different Ni_xCo_{10-x} (x = 1–8) catalysts at different temperatures.

Graphene is an ideal supporting material as previously mentioned, and Ni_1Co_9 is an amorphous catalyst that can easily become agglomerated. The introduction of graphene as a supporting material does not affect the intrinsic performance of the catalyst; rather, it improves the catalyst specific surface area. As Fig. 2(a) shows, Ni_1Co_9 with graphene exhibited better performance, especially an increase in reaction rate. Subsequently, a durability test of Ni_1Co_9@GP for $NaBH_4$ hydrolysis was conducted, and the results are illustrated in Fig. 2(b). Even after ten cycles of catalytic hydrolysis, the catalytic activity of Ni_1Co_9@GP decreased only slightly, so that Ni_1Co_9@GP could still maintain a high catalytic activity. According to the result, Ni_1Co_9@GP had a relatively high stability compared with the other A_xB_{10-x}@GP catalysts in $NaBH_4$ hydrolysis at 303 K.

The XRD patterns of Ni_1Co_9@GP are shown in Fig. 3(a). Few differences existed between the Ni_1Co_9 and Ni_1Co_9@GP catalysts, which indicates that introducing graphene did not change Ni_1Co_9 structure. As shown in Fig. 3(b), the Ni_1Co_9 exhibited a lamellar structure, and graphene acted as a supporting "paper" to enlarge the specific surface area of the Ni_1Co_9 and make some of the alloy particles evenly distributed on the support material. Herein, graphene can be an ideal material to enhance catalyst contact area and stability.

Additionally, the Brunauer–Emmett–Teller (BET) surface areas and pore volumes of Ni_1Co_9 and Ni_1Co_9@GP were obtained by N_2 adsorption and desorption at 77 K. As can be seen in Fig. 4(a), the samples of transition metal alloys with graphene support had higher surface areas and larger pore volumes than the alloys only, which may increase the active sites and contact area between the catalysts and hydrides. Notably, the BET surface area and pore volume of Ni_1Co_9 were evaluated to be 81.1 $m^2 \cdot g^{-1}$ and 3.8 nm, respectively, while those of Ni_1Co_9@GP were 128.4 $m^2 \cdot g^{-1}$ and 3.8 nm, respectively.

To obtain information on the surface element valence states of Ni_1Co_9@GP, which had the best catalytic performance among all the Ni_xCo_{10-x}@GP, characterization using XPS was performed, and the results are shown in Fig. 5. In the Ni 2p XPS spectrum, the two peaks with binding energies of 852.9 and 870.2 eV can be assigned to Ni(0) $2p_{3/2}$ and Ni(0) $2p_{1/2}$, respectively. However, there are two lower intensity peaks at 853.6 and 871.2 eV which can be assigned to Ni(II) $2p_{3/2}$ and Ni(II) $2p_{1/2}$, respectively. The XPS spectra of Co $2p_{3/2}$ and Ni 2p in Ni_1Co_9@GP are presented in Fig. 5. The figure shows that the C 1s spectrum can be divided into

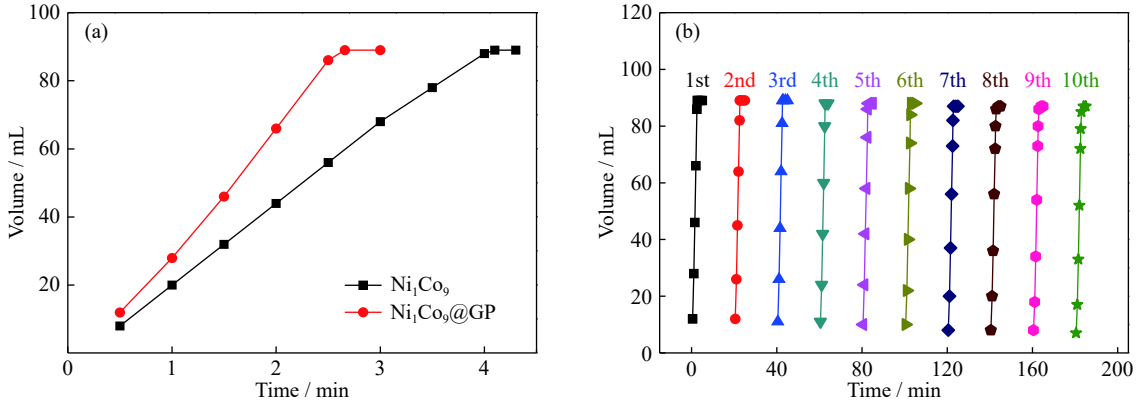

Fig. 2. (a) Catalytic test of Ni_1Co_9 and Ni_1Co_9@GP and (b) durability tests of Ni_1Co_9@GP for $NaBH_4$ hydrolysis at 303 K.

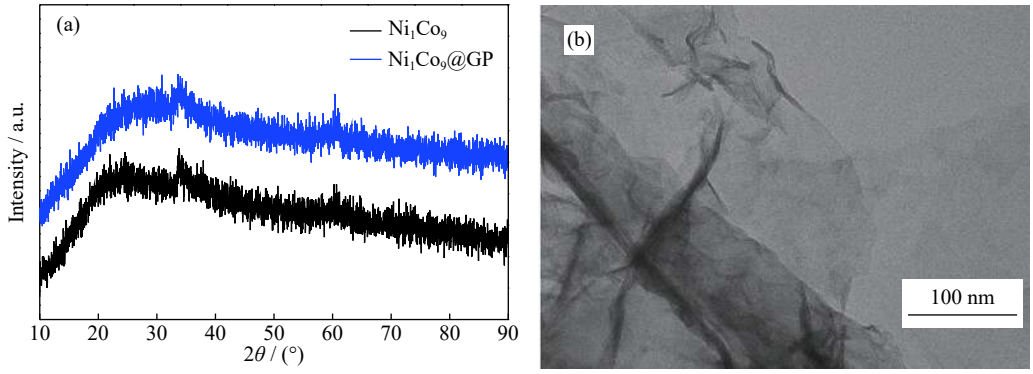

Fig. 3. XRD patterns (a) and TEM image (b) of of Ni_1Co_9@GP.

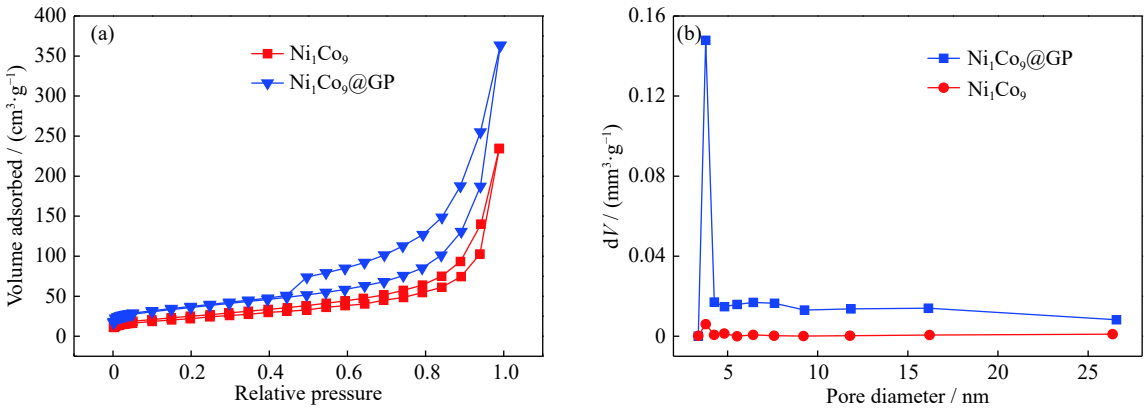

Fig. 4. N_2 adsorption–desorption isotherms (a) and pore size distribution (b) of Ni_1Co_9 and Ni_1Co_9@GP.

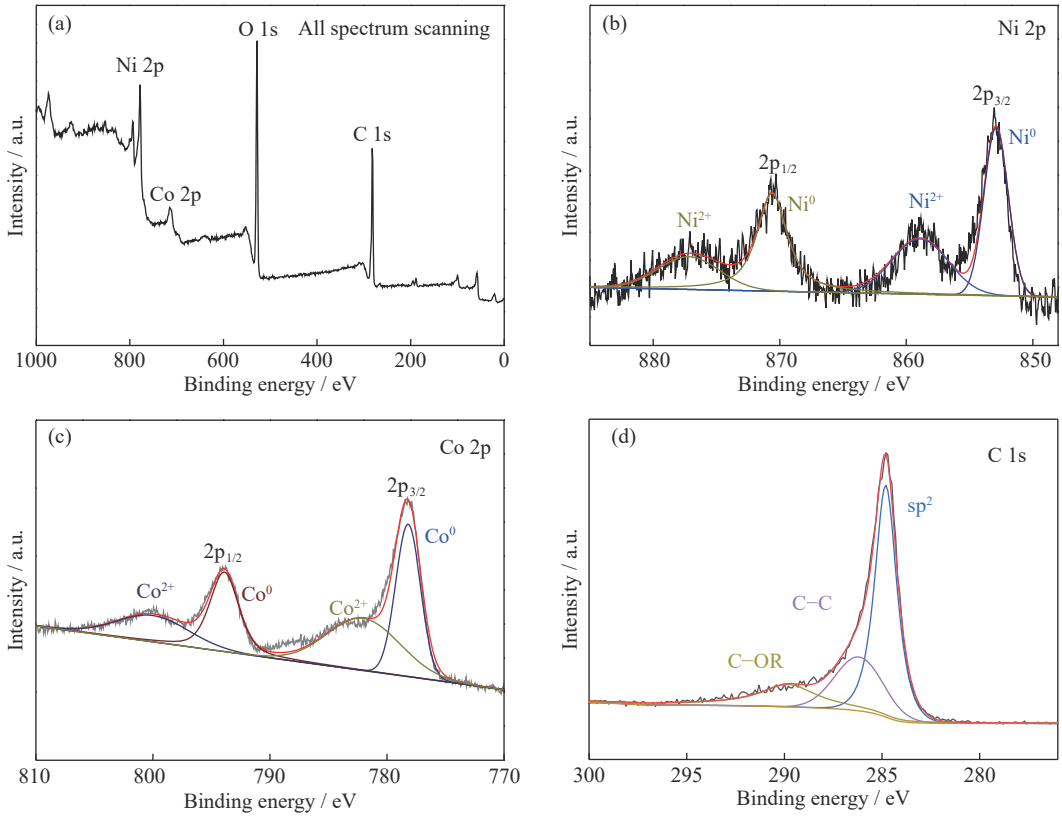

Fig. 5. XPS wide-scan spectra (a) and detailed spectra of (b) Ni 2p, (c) Co 2p, and (d) C 1s in Ni_1Co_9@GP.

three peaks, which are situated at 284.8 eV (sp^2 C), 286.2 eV (C–OR), and 289.8 eV (C–C).

Considering that the molar mass of binary transition metals can affect the catalytic performance, three catalysts, all with 20 mg graphene but with different molars of 0.13, 0.26, and 0.39 mmol, were chosen to catalyze the hydrolysis of $NaBH_4$. As shown in Fig. 6, the 0.39 mmol Ni_1Co_9@GP reached equilibrium more quickly than the others. Therefore, the 0.39 mmol Ni_1Co_9@GP was the best catalyst among the three.

As can be seen in Fig. 7(a), the $NaBH_4$–H_2O was replaced with $NaBH_4$–D_2O. To find out where the extra four hydrogen atoms came from, this experiment was H_2O-free. In this case, the volume of the H_2–D_2 mix gas was finally 89 mL, which indicates that extra four hydrogen atoms came from H_2O. In Fig. 7(b), the slope was 0.708, indicating that the hydrolysis of $NaBH_4$ by Ni_1Co_9@GP was a first-order reaction in terms of the nanocatalyst concentration.

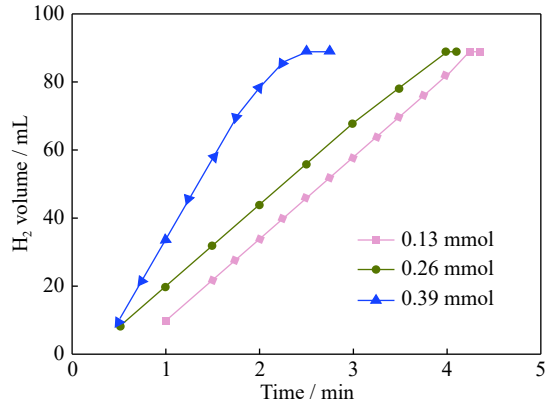

Fig. 6. Hydrolysis of $NaBH_4$ with Ni_1Co_9@GP catalysts in different molars.

The Ni_1Co_9@GP outperformed most of the similar catalysts, according to Table 1. Furthermore, it is much easier to prepare than other catalysts for the hydrolysis of $NaBH_4$.

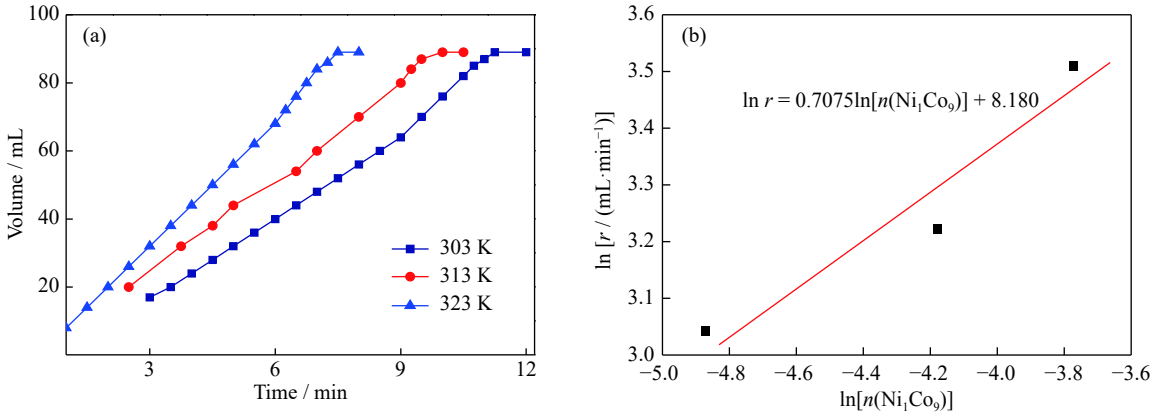

Fig. 7. (a) Time plots of the hydrolysis of $NaBH_4$–D_2O catalyzed by Ni_1Co_9@GP at 303, 313, and 323 K; (b) plots of hydrolysis rate (r) vs. time for various molar mass (n) of Ni_xCo_{10-x}.

Table 1. Comparison of recent literature results on Co-based catalysts for the hydrolysis of $NaBH_4$

Catalyst	TOF / ($mL \cdot min^{-1} \cdot g^{-1}$)	Temperature / °C	Ref.
CoNPs@ZIF-8	14023/19476	40	[6]
Ni_1Co_3/AC	658.8	50	[9]
Co–B NPs	26000	25	[27]
Ni–Co–B/Cu sheet	14778	25	[28]
Co–B/Ni foam	11000	30	[29]
Fe–Co–B/Ni foam	22000	30	[30]
Co–B/ZIF-8	563	50	[31]
NiFePd/MIL-101	7800	50	[32]
Ni–Co/r–GO	1280	90	[26]
Ni_1Co_9/GP	25534	30	This study

4. Conclusion

A hydrothermal experiment process was used to synthesize A_xB_{10-x}@GP (A, B = nickel, cobalt, copper, iron, and molybdenum). The introduced GP not only greatly increased the surface area of these catalysts but acted as a host material to maintain the metal particles evenly distributed from aggregating. In addition, catalytic performance tests proved that the

morphology of the catalyst, as well as the supporting material, can influence the final performance. Among the Ni_xCo_{10-x}@GP catalysts, which are based on cheap and earth-abundant transition metals, the Ni_1Co_9@GP showed the best TOF value, 603.82 mL·mmol^{-1}·min^{-1}, at 303 K, in the hydrolysis process. The high specific area and even distribution of the NPs endowed the Ni_1Co_9@GP with high catalytic activity and stability. As a result, our finding is a simple, safe, environment-friendly, and economic method to prepare nanocatalysts and can pave a new way to obtain similar efficient catalysts.

Acknowledgement

This work was financially supported by the National Natural Science Foundation of China (No. 51602293) and Sichuan Provincial Science and Technology support project (No. 2020YFG0102).

References

[1] R. Chamoun, U.B. Demirci , and P. Miele, Cyclic dehydrogenation–(re)hydrogenation with hydrogen-storage materials: An overview, *Energy. Technol.*, 3(2015), No. 2, p. 100.

[2] D.M.F. Santos and C.A.C. Sequeira, Sodium borohydride as a fuel for the future, *Renewable Sustainable Energy Rev.*, 15(2011), No. 8, p. 3980.

[3] U.B. Demirci, Impact of H.I. Schlesinger's discoveries upon the course of modern chemistry on B−(N−)H hydrogen carriers, *Int. J. Hydrogen Energy*, 42(2017), No. 33, p. 21048.

[4] P.Y. Olu, A. Bonnefont, G. Braesch, V. Martin, E.R. Savinova, and M. Chatenet, Influence of the concentration of borohydride towards hydrogen production and escape for borohydride oxidation reaction on Pt and Au electrodes—Experimental and modelling insights, *J. Power Sources*, 375(2018), p. 300.

[5] H.L. Wang, J.M. Yan, Z.L. Wang, S.I. O, and Q. Jiang, Highly efficient hydrogen generation from hydrous hydrazine over amorphous $Ni_{0.9}Pt_{0.1}/Ce_2O_3$ nanocatalyst at room temperature, *J. Mater. Chem. A*, 1(2013), No. 47, p. 14957.

[6] C. Luo, F.Y. Fu, X.J. Yang, J.Y. Wei, C.L. Wang, J. Zhu, D.S. Huang, D. Astruc, and P.X. Zhao, Highly efficient and selective Co@ZIF-8 nanocatalyst for hydrogen release from sodium borohydride hydrolysis, *ChemCatChem*, 11(2019), No. 6, p. 1643.

[7] B. Šljukić, D.M.F. Santos, C.A.C. Sequeira, and C.E. Banks, Analytical monitoring of sodium borohydride, *Anal. Methods*, 5(2013), No. 4, p. 829.

[8] J.H. Sinfelt, Catalysis by alloys and bimetallic clusters, *Acc. Chem. Res.*, 10(1977), No. 1, p. 15.

[9] A. Didehban, M. Zabihi, and J.R. Shahrouzi, Experimental studies on the catalytic behavior of alloy and core-shell supported Co–Ni bimetallic nano-catalysts for hydrogen generation by hydrolysis of sodium borohydride, *Int. J. Hydrogen Energy*, 43(2018), No. 45, p. 20645.

[10] H. Esmaili, A. Kotobi, S. Sheibani, and F. Rashchi, Photocatalytic degradation of methylene blue by nanostructured Fe/FeS powder under visible light, *Inter. J. Miner. Metall. Mater.*, 25(2018), No. 2, p. 244.

[11] G.J. Hutchings and C.J. Kiely, Strategies for the synthesis of supported gold palladium nanoparticles with controlled morphology and composition, *Acc. Chem. Res.*, 46(2013), No. 8, p. 1759.

[12] M. Takahashi, H. Koizumi, W.J. Chun, M. Kori, T. Imaoka, and K. Yamamoto, Finely controlled multimetallic nanocluster catalysts for solvent-free aerobic oxidation of hydrocarbons, *Sci. Adv.*, 3(2017), No. 7, art. No. e1700101.

[13] S.N. Li, R.X. Ma, and C.Y. Wang, Solid-phase synthesis of Cu_2MoS_4 nanoparticles for degradation of methyl blue under a halogen-tungsten lamp, *Int. J. Miner. Metall. Mater.*, 25(2018), No. 3, p. 310.

[14] R. Ferrando, J. Jellinek, and R.L. Johnston, Nanoalloys: From theory to applications of alloy clusters and nanoparticles, *Chem. Rev.*, 108(2008), p. 845.

[15] F.F. Chen, K. Shen, J.Y. Chen, X.F. Yang, J. Cui, and Y.W. Li, General immobilization of ultrafine alloyed nanoparticles within metal-organic frameworks with high loadings for advanced synergetic catalysis, *ACS Cent. Sci.*, 5(2019), No. 1, p. 176.

[16] Y.P. Guo and G.X. Lu, Graphene supported Co–Mo–P catalyst for efficient photocatalyzed hydrogen generation, *Int. J. Hydrogen Energy*, 41(2016), No. 16, p. 6706.

[17] D. Wang, J. Liu, J.B. Xi, J.Z. Jiang, and Z.W. Bai, Pd–Fe dual-metal nanoparticles confined in the interface of carbon nanotubes/N-doped carbon for excellent catalytic performance, *Appl. Surf. Sci.*, 489(2019), p. 477.

[18] Z.K. Cui, Y.P. Guo, and J.T. Ma, In situ synthesis of graphene supported Co–Sn–B alloy as an efficient catalyst for hydrogen generation from sodium borohydride hydrolysis, *Int. J. Hydrogen Energy*, 41(2016), No. 3, p. 1592.

[19] F. Li, Q.M. Li, and H. Kim, CoB/open-CNTs catalysts for hydrogen generation from alkaline $NaBH_4$ solution, *Chem. Eng. J.*, 210(2012), p. 316.

[20] W.L. Niu, D.B. Ren, Y.Y. Han, Y.J. Wu, and X.L. Gou, Optimizing preparation of carbon supported cobalt catalyst for hydrogen generation from $NaBH_4$ hydrolysis, *J. Alloys Compd.*, 543(2012), p. 159.

[21] H.R. Xue, J. Tang, H. Gong, H. Guo, X.L. Fan, T. Wang, J.P. He, and Y. Yamauchi, Fabrication of PdCo bimetallic nanoparticles anchored on three-dimensional ordered N-doped porous carbon as an efficient catalyst for oxygen reduction reaction, *ACS Appl. Mater. Interfaces*, 8(2016), No. 32, p. 20766.

[22] Y. Liang, H.B. Dai, L.P. Ma, P. Wang, and H.M. Cheng, Hydrogen generation from sodium borohydride solution using a ruthenium supported on graphite catalyst, *Int. J. Hydrogen Energy*, 35(2010), No. 7, p. 3023.

[23] L. Zhang, Z.X. Xie, and J.L. Gong, Shape-controlled synthesis of Au–Pd bimetallic nanocrystals for catalytic applications, *Chem. Soc. Rev.*, 45(2016), p. 3916.

[24] A. Wong, Q. Liu, S. Griffin, A. Nicholls, and J.R. Regalbuto, Synthesis of ultrasmall, homogeneously alloyed, bimetallic nanoparticles on silica supports, *Science*, 358(2017), No. 6369, p. 1427.

[25] Y.G. Yao, Z.N. Huang, P.F. Xie, S.D. Lacey, R.J. Jacob, H. Xie, F.J. Chen, A.M. Nie, T.C. Pu, M. Rehwoldt, D.W. Yu, M.R. Zachariah, C. Wang, R. Shahbazian-Yassar, J. Li, and L.B. Hu, Carbothermal shock synthesis of high-entropy-alloy nanoparticles, *Science*, 359(2018), No. 6383, p. 1489.

[26] S. Saha, V. Basak, A. Dasgupta, S. Ganguly, D. Banerjee, and K. Kargupta, Graphene supported bimetallic G–Co–Pt nanohybrid catalyst for enhanced and cost effective hydrogen generation, *Int. J. Hydrogen Energy*, 39(2014), No. 22, p. 11566.

[27] C.C. Chou, C.H. Hsieh, and B.H. Chen, Hydrogen generation

from catalytic hydrolysis of sodium borohydride using bimetallic Ni–Co nanoparticles on reduced graphene oxide as catalysts, *Energy*, 90(2015), p. 1973.

[28] B.H. Liu and Q. Li, A highly active Co–B catalyst for hydrogen generation from sodium borohydride hydrolysis, *Int. J. Hydrogen Energy*, 33(2008), No. 24, p. 7385.

[29] Y.S. Wei, W. Meng, Y. Wang, Y.X. Gao, K.Z. Qi, and K. Zhang, Fast hydrogen generation from $NaBH_4$ hydrolysis catalyzed by nanostructured Co–Ni–B catalysts, *Int. J. Hydrogen Energy*, 42(2017), No. 9, p. 6072.

[30] H.B. Dai, Y. Liang, P. Wang, and H.M. Cheng, Amorphous cobalt-boron/nickel foam as an effective catalyst for hydrogen generation from alkaline sodium borohydride solution, *J. Power Sources*, 177(2008), No. 1, p. 17.

[31] Y. Liang, P. Wang, and H.B. Dai, Hydrogen bubbles dynamic template preparation of a porous Fe–Co–B/Ni foam catalyst for hydrogen generation from hydrolysis of alkaline sodium borohydride solution, *J. Alloys Compd.*, 491(2010), No. 1-2, p. 359.

[32] Q.M. Li, W. Yang, F. Li, A.L. Cui, and J. Hong, Preparation of CoB/ZIF-8 supported catalyst by single step reduction and its activity in hydrogen production, *Int. J. Hydrogen Energy*, 43(2018), No. 1, p. 271.